Regular Article

PHYSICAL CHEMISTRY RESEARCH
Published by the
Iranian Chemical Society
www.physchemres.org
info@physchemres.org

Phys. Chem. Res., Vol. 11, No. 1, 63-78, March 2023
DOI: 10.22036/pcr.2022.321821.2009

Optimization of Adsorption Process Parameters of Allura Red Removal Using Nanodiopside/Zn-Fe Layered Double Hydroxide Composite by Response Surface Methodology: A Kinetic, Thermodynamic, and Equilibrium Approach

N. Sohrabi*, M. Hemmasi and N. Rasuli
Department of Chemistry, Payame Noor University (PNU), P. O. Box: 19395-3697, Tehran, Iran
(Received 27 December 2021, Accepted 9 May 2022)

To optimize the Allura Red adsorption parameters by nanodiopside/zinc-iron layered double hydroxide composite, response surface methodology was employed. The optimization was carried out to ensure high performance in the experimental ranges employed and compare the conjunct effects of the initial concentration of Allura Red, pH, adsorbent dosage, temperature, and contact time on the adsorption process. A total of 32 adsorption experimental runs were carried out following the detailed conditions designed by response surface methodology based on the Box-Behnken design to optimize the status employed in the batch process. Analysis of variance (ANOVA) showed that a second-order polynomial regression equation was the most appropriate polynomial regression for fitting the experimental data. The experimental verification tests showed an agreement between the predicted and experimental responses (R^2). The optimal point obtained was located in the valid region and the optimum adsorption parameters were approximated at an initial concentration of 19.80 mg l^{-1} for Allura Red, a pH value of 4.09, an adsorbent dosage of 0.04 g, a temperature of 32.61 °C, and a contact time of 23.93 min.

Keywords: Response surface, Adsorption, Allura Red, Nanodiopside, Layered double hydroxide

INTRODUCTION

Nowadays, foundational research and practical application of such research are aimed at removing dyes from wastewater [1,2]. It is difficult to treat the wastewater that contains dyes and metals by conventional methods [3-6]. Thus, developing an attainable, feasible, and reliable method to exploit sorption techniques is necessary. Several biological and physicochemical methods, such as sorption techniques, coagulation, precipitation, ion exchange, filtration, electrolysis, and biological treatments, have been suggested for transferring dyes [7]. Due to its efficiency, economic feasibility, simplicity of design, recycling potential, and lack of secondary pollution, the removal of dye from aqueous solutions *via* sorption has received much attention recently [8,9]. However, finding an efficient adsorbent for the fundamental and practical application of adsorption is a key challenge.

Disodium 6-hydroxy-5-((2-methoxy-5-methyl-4-sulfophenyl)azo)-2-naphthalenesulfonate, Allura Red, is a hazardous dye that is widely used for coloring paper, textiles, leather, wood, and food additives. It has also been confirmed that a higher concentration of Allura Red can result in carcinogenic, allergic, and respiratory problems by adversely affecting both human and animal health [10]. Adsorption of a Variety of Dyes onto Layered Double Hydroxide (LDH)

LDHs have been reported recently n the literature [11-14]. LDHs are anionic clays with high adsorption capacity, especially for dyes [15-17]. Although LDHs have a high adsorption capacity to adsorb dyes, their technical application scopes is restricted due to their low separation

*Corresponding author. E-mail: sohrabnas99@gmail.com

efficiency in aqueous solution.

Diopside is a pyroxene mineral, a relevant bioactive substrate [18,19], and is known as a silicate phase. It is a material worthy of attention due to its excellent mechanical and biological properties, low cost, low degradation, and good biocompatibility [20]. Nanodiopside has several surface properties, such as homogenous morphology, particle size, and porosity; its high surface area is the main reason why it has been considered a good absorbent candidate for the removal of pollutants [21]. As a result, in this study, the nanodiopside/Zn-FeLDH composite was used as a novel, green, and natural adsorbent for the removal of Allura red, which is an azo dye pollutant.

In this study, the mathematical relationship between the efficiency of the removal of Allura Red and the influence of operational parameters, including pH, temperature, Allura Red concentration, contact time, and adsorbent dose, was determined using response surface methodology (RSM) [22,23]. The RSM is based on the most appropriate choice of factors and levels and offers useful ideas about the main interaction of parameters based on a minimum number of experiments, which, in turn, can guide researchers to find the best real optimum point instead of localized imaginary points [24]. RSM uses an experimental design, such as the central composite design (CCD) and the Box-Behnken design (BBD), to fit a model by the least-squares method [24]. In the present study, the effect of different parameters on the efficiency of the removal of Allura Red was investigated using the CCD. The use of this method has been reported before in several biocompatible materials [26-28]

EXPERIMENTAL

Materials and Methods

The Allura Red dye used in this research was supplied by Merck Company (Darmstadt, Germany). To prepare the working solution of Allura Red, its stock solution (200 mg l^{-1}) was prepared and then the daily necessary solutions were prepared using its subsequent dilution. The adsorbent dosage of 0.04 g and the initial Allura Red concentration of 19.80 g l^{-1} were considered. A digital pH meter (Methrohm) was employed to adjust the pH. The SEM was performed on Hitachi, model S-4160. UV-Vis spectra were recorded with a maximum wavelength at 504 nm on a Lambda 2 Perkin Elmer spectrophotometer and a BET surface area using a BELSORP Mini II. Fourier-transform infrared spectroscopy (FT-IR) absorption spectra of Allura Red were recorded using KBr disk by an FT-IR spectrometer (model 460 plus) in the region of 4000-400 cm^{-1}. All chemicals handled in this study were of analytical grade and were used beyond further purification treatment.

Preparation of Nanodiopside-LDH Composite

In this research, magnesium chloride ($MgCl_2.6H_2O$), calcium nitrate ($Ca(NO_3)_2.4H_2O$)), pure ethanol (C_2H_5OH), sodium hydroxide (NaOH), cadmium nitrate ($Cd(NO_3)_2.4H_2O$)), tetraethyl orthosilicate ($C_8H_2OSiO_4$), sodium chloride (NaCl), hydrochloric acid (HCl), and nitric acid (HNO_3) were used to prepare nanodiopside/Zn-Fe LDH composite, as an adsorbent. Diopside powders were synthesized by the sol-gel method and exploiting tetraethyl orthosilicate ($(C_2H_5O)_4Si$, (TEOS)), magnesium nitrate hexahydrate ($Mg(NO_3)_2.6H_2O$), and calcium nitrate. First, 0.125 mol of $Ca(NO_3)_2.4H2O$ and $MgCl_2.6H_2O$ were dissolved in ethanol; then, the solution was stirred vigorously for 30 min at 80 °C to be dissolved in the solvent. $Si(OC_2H_5)_4$ (TEOS) was added to the homogenous solution and slowly stirred to prepare a wet gel. After having been dried in an oven at 100 °C for 24 h, the resulting dried powder was ground in a hand mortar, followed by calcination at 700 °C for 2 h and at 1100 °C for another 24 h. Finally, the powder was mechanically ball-milled using a zirconia ball mill (Daehan Science, Seoul, Korea) for 8 h to accumulate nanodiopside particles in the range of 100 nm. Then, 2.4 g nanodiopside was dissolved in water, and the aqueous solution, containing 1.44 mmol $Zn(NO_3)_2.6H_2O$ and 0.48 mmol $Fe(NO_3)_3.9H_2O$, was added dropwise to the suspension of nanodiopside under vigorous stirring. The solution pH maintained at pH 7 and heated in an oven (60 °C) for 2 h. The synthesized nanodiopside/Zn-Fe LDH was collected from the reaction mixture by centrifuge [29].

Characterization

In order to check the level properties of nanodiopside/Zn-Fe LDH composite, FT-IR spectra

(JASCO, 680 PLUS) were obtained on a JASCO 680-plus in the range of 400-4000 cm^{-1} using KBr pellets. In addition, the prepared samples were examined by X-ray powder diffraction (XRD). An X-ray diffractometer with Cu Kα radiation at a scan rate of 0.02 min was used for the crystallographic structural analysis of the sample (model Asenware AW-XDM300). Specific surface area, cumulative pore volume, and pore size distribution were determined using Brunauer-Emmett-Teller (BET), on a Quantachrome ChemBET-3000, and Barrett-Joyner-Halenda (BJH) methods. The field emission SEM (FESEM) is equipped with EDX microanalysis and is capable of detecting the slightest phases (Model MIRA 3-XMU).

Adsorption Studies

The dye concentrations were determined according to the general traditional spectrophotometer method at its maximum wavelength (504 nm) over working concentration range. The efficiency of Allura Red removal was determined at different experimental conditions specified according to the CCD method. The isotherm studies were carried out in the range of 10-30 mg l^{-1} to obtain adsorption isotherms. The dyes removal percentages were calculated using the following equation:

$$\%Allura\ \mathrm{Re}d\ removal = \frac{(C_0 - C_t)}{C_0} \times 100 \quad (1)$$

where C_0 (mg l^{-1}) and C_t (mg l^{-1}) are the concentration of the target at initial and after time t, respectively. The adsorbed dye amount (q_e (mg g^{-1})) was calculated by the following equation:

$$q_e = \frac{(C_0 - C_t)V}{W} \quad (2)$$

where C_0 and C_e (mg l^{-1}) are the initial and equilibrium dye concentrations in the aqueous solution, respectively, V (l) is the volume of the solution, and W (g) is the mass of the adsorbent.

Response Surface Methodology (RSM)

RSM was used to optimize five variables, including the initial concentration of Allura Red, pH, adsorbent dosage, temperature, and contact time. These five variables were chosen as independent variables. The amount of Allura Red removed (mg g^{-1}) was set as the output response variable. The ranges and levels of the variables utilized are presented in Table 2. Design-Expert software 7.1.5 was used for response surface modeling, statistical analysis, and optimization. The combined effects of those five variables were investigated using the CCD. Thirty-two sets of experiments, including six replications, were performed (Table 3). The data were analyzed using analysis of variance (ANOVA), and the optimal values of the Allura Red removal were estimated using 3D response surface plots.

RESULTS AND DISCUSSION

Characterization

In the FT-IR spectra of the nanodiopside bands (Fig. 1a) in the 4000-400 cm^{-1} spectral range, bands in the region of 676 cm^{-1} can be attributed to the bending vibrations, and bands in the region of 850-1100 cm^{-1} can be attributed to the symmetric stretching vibrations of the silicate structure. These bands can be ascribed to the Si-O symmetric stretching of bridging and non-bridging oxygen atoms, Si-O-Si symmetric stretching, and Si-O-Si asymmetric stretching [21,29]. The important absorption bands for Zn-Fe LDH are usually around 3500 cm^{-1}, which has been assigned to the stretching mode of OH groups in the LDH structure, interlayer water, and physic adsorbed water [30]. After the nanodiopside was combined with Zn-Fe LDH in the nanocomposite, the obtained FT-IR spectra exhibited mixed bands between the individual components. The process was also characterized by the appearance and disappearance of some characteristic absorption bands. There was a clear reduction in the intensity of the absorbance bands around 3500 cm^{-1}, which can be attributed to the overlap of the 3429 cm^{-1} peak of nanodiopside and O\\H stretching of absorbed water [31]. The FT-IR spectra of free nanodiopside and nanodiopside/Zn-Fe LDH composite are shown in Figs. 1a and 1b, respectively.

Moreover, the SEM images of nanodiopside and nanodiopside/Zn-Fe LDH composite were studied and the results are shown in Fig. 2. It is evident that the surface

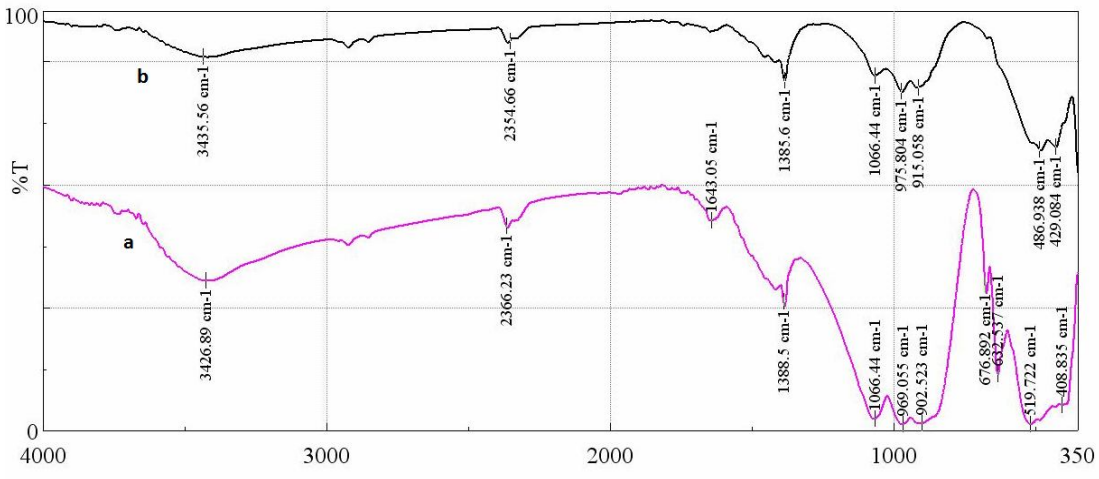

Fig. 1. The FT-IR spectra of (a) nanodiopside and (b) nanodiopside/Zn-Fe LDH composite.

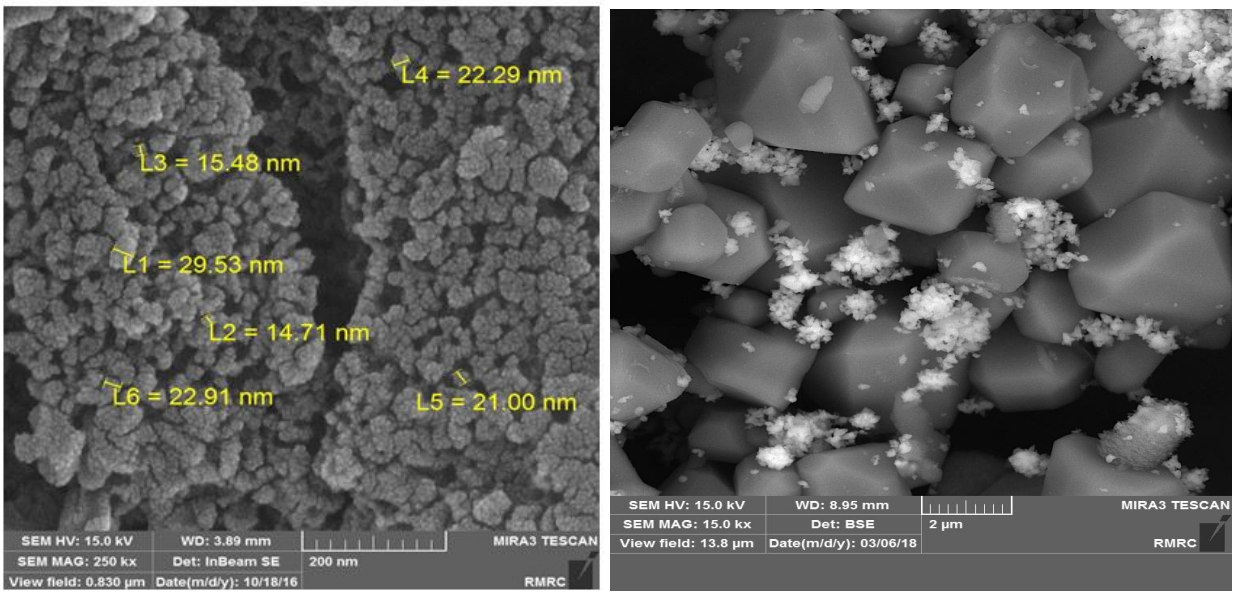

Fig. 2. The SEM images of (a) nanodiopside and (b) nanodiopside/Zn-Fe LDH composite.

morphology of nanodiopside/Zn-Fe LDH composite is different from that of the nanodiopside sample.

In this research, the BET method was used. The interference by the surrounding phase is especially problematic for the BET N_2-adsorption/desorption isotherm method because the entire surface is modified by vacuum treatment before N_2-adsorption. The surface properties of the adsorbent are presented in Table 1 and Fig. 3. According to the BET analysis, the specific surface area of nanodiopside/Zn-Fe LDH composite was 2.7308 m^2 g^{-1}. Also, the total pore volume and the average pore diameter of nanodiopside/Zn-Fe LDH were 0.0190 cm^3 g^{-1} and 27.85 nm, respectively. In addition, the results reflected adsorption isotherms of type III, which occurs when the adsorbate-adsorbate interaction is big compared to the adsorbate-adsorbent interaction [32].

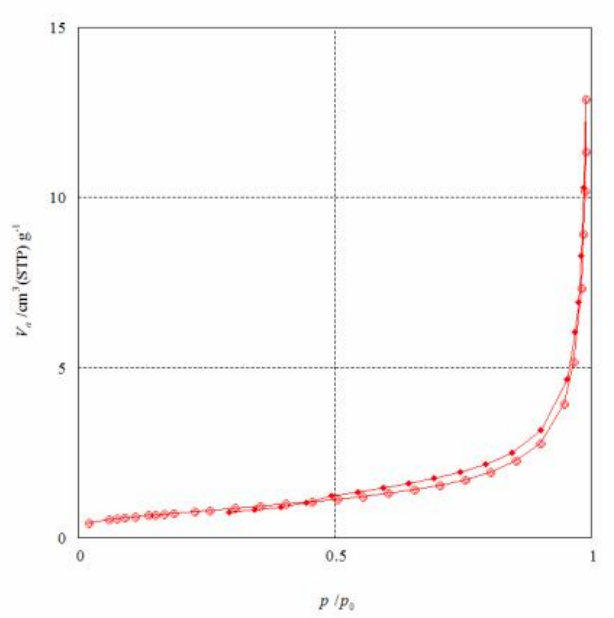

Fig. 3. The results of adsorption-desorption measurement (BET method) of nanodiopside/Zn-Fe LDH.

Figure 4 shows the EDS spectrum of the prepared sample. This figure shows the presence of relevant elements and the purity of the synthesized nanodiopside/Zn-Fe LDHcomposite.

Central Composite Design (CCD)

As shown in Table 2, five independent variables were studied and classified into three levels, namely, low, central, and high, with the coded values of +1, 0, and -1, respectively. Furthermore, the star points of +2 and -2 for +α and -α, respectively, were selected for each set of experiments. Along with this method, ANOVA was used to investigate the main interaction and quadratic effects of all variables.

A p-value less than 0.05 in Table 5 shows the statistical importance of an effect at a 95% confidence level. F-test was used to evaluate the statistical significance of each term in the polynomial equation within a 95% confidence interval. Data analysis resulted in a semi-empirical expression of the extraction recovery (ER%) using the following equation:

Table 1. The Results of Surface Area and Porosity Measurement (BET Method) of Nanodiopside/Zn-Fe LDH

Sample	Specific surface Area (m^2 g^{-1})	Micropore vol. (cm^3 g^{-1})	Micropore size (nm)
Nanodiopside/Zn-Fe LDH composite	2.730	0.0190	27.85
Nanodiopside	149.501	0.199	1.25

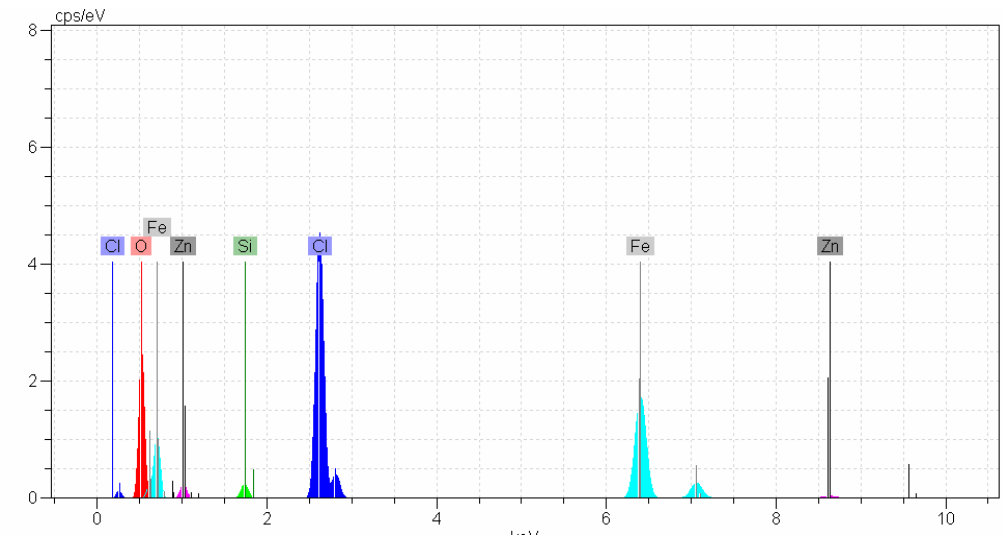

Fig. 4. The EDS spectrum of the synthesized nanodiopside/Zn-Fe LDH composite.

Table 2. Experimental Factors and Levels in the Central Composite Design

Factors	Unit	Symbol	Levels				
			-α	Low (-1)	Central (0)	High (+1)	+α
Concentration	mg l^{-1}	A	5	11.25	17.5	23.75	30.00
pH		B	2.5	3.125	3.75	4.37	5.00
Adsorbent dosage	mg	C	0.009	0.029	0.050	0.075	0.100
Temperature	°C	D	25	27.5	30	32.5	35.00
Contact time	min	E	10	15	20	25	30.00

Table 3. Central Composite Design with the Observed and Predicted Values for the Variables Related to the Removal Efficiency (%) of Allura Red

Std order	Run order	Blocks	Initial concentration	pH	Adsorbent dosage	Temperature	Contact time	Response
30	1	1	17.5	3.75	0.05	30	20	98.14
3	2	1	5	5	0.01	25	10	96.74
16	3	1	30	5	0.1	35	30	96.54
13	4	1	5	2.5	0.1	35	30	95.88
20	5	1	17.5	6.25	0.05	30	20	98.56
14	6	1	30	2.5	0. 1	35	10	98.04
31	7	1	17.5	3.75	0.05	30	20	98.1
29	8	1	17.5	3.75	0.05	30	20	98.13
2	9	1	30	2.5	0.01	25	10	99.70
23	10	1	17.5	3.75	0.05	30	20	98.49
12	11	1	30	5	0.01	35	10	97.78
27	12	1	17.5	3.75	0.05	30	20	98.14
5	13	1	5	2.5	0.1	25	10	96.68
17	14	1	17.5	3.75	0.05	30	20	98.12
22	15	1	17.5	3.75	0.15	30	20	97.22
10	16	1	30	2.5	0.01	35	30	99.19
19	17	1	17.5	1.25	0.05	30	20	98.49
9	18	1	5	2.5	0.01	35	10	99.44
18	19	1	42.5	3.75	0.05	30	20	97.74
26	20	1	17.5	3.75	0.05	30	40	97.47
11	21	1	5	5	0.01	35	30	95.36
1	22	1	5	2.5	0.01	25	30	99.26
25	23	1	17.5	3.75	0.05	30	20	96.69
7	24	1	5	5	0.1	35	10	91.4
6	25	1	30	2.5	0.1	25	30	98
8	26	1	30	5	0.1	25	10	96.15
28	27	1	17.5	3.75	0.05	30	20	98.11
15	28	1	5	5	0.1	35	10	*95*
4	29	1	30	5	0.01	25	30	97.75
32	30	1	17.5	3.75	0.05	30	20	98.14
24	31	1	17.5	3.75	0.05	40	20	98.14
21	32	1	17.5	3.75	0.04	30	20	97.53

Table 4. Model Summary Statistics

Source	Std. Dev.	R-Squared	Adjusted R-Squared	Predicted R-Squared	PRESS	
Linear	1.47	0.4806	0.3807	0.1625	602.26	
2FI	1.36	0.6127	0.2497	-6.1614	549.21	
Quadratic	1.24	0.9991	0.9721	0.9659	64.23	Suggested

Table 5. The Results of ANOVA for Response Surface Quadratic Model of Nanodiopside

Source	Sum of squares	df	Mean square	F-value	p-Value	
Model	53.04	20	1.23	1.23	0.0369	Significant
A	6.65	1	3.09	3.09	0.0106	
B	15.58	1	7.25	7.25	0.0210	
C	13.72	1	6.38	6.38	0.0028	
D	0.031	1	0.014	0.014	0.09073	
E	0.88	1	0.41	0.41	0.5354	
AB	2.28	1	2.28	1.06	0.3249	
AC	2.37	1	2.37	1.10	0.3164	
AD	0.17	1	0.17	0.079	0.7844	
AE	2.08	1	2.08	0.97	0.3468	
BC	0.012	1	0.012	5.731E-003	0.9410	
BD	0.87	1	0.87	0.40	0.5384	
BE	0.59	1	0.59	0.28	0.6094	
CD	1.51	1	1.51	0.70	0.4197	
CE	0.24	1	0.24	0.11	0.7450	
DE	0.012	1	0.012	5.527E-003	0.9421	
A^2	0.62	1	0.62	0.29	0.6017	
B^2	3.098E-004	1	3.098E-004	1.441E-004	0.9906	
C^2	2.37	1	2.37	1.10	0.3162	
D^2	0.071	1	0.071	0.033	0.8590	
E^2	3.76	1	3.76	1.75	0.2129	
Residual	23.65	11	2.15			
Lack of fit	*22.78*	6	3.80	21.86	0.0619	Not significant
Pure error	0.87	5	0.17			
Cor total	76.69	31				
Adeq	5.724					

Table 6. Optimized Adsorption Parameters

Concentration (mg l^{-1})	pH	Adsorbent dose (g)	Temperature (°C)	Time (min)
19.80	4.09	0.04	32.61	23.93

Y = +98.10 +0.53A -0.81B -0.76C +0.036D -0.19E +0.38AB +0.38AC -0.10AD +0.36AE +0.028BC +0.23BD -0.19BE +0.31CD -0.12CE -0.027DE -0.15A2 +3.250E -003B2 -0.28C2 -0.049D2 -0.36E2,

in which Y is the amount of Allura Red (mg g^{-1}), A is the initial concentration of Allura Red (mg l^{-1}), B is the pH, C is the adsorbent dosage (mg), D is the temperature (°C), and E is the contact time (min).

The acceptable quality of the polynomial model fit was expressed with the coefficient of determination (squared R^2 = 0.9991 and adjusted R^2 = 0.9721). The plot of experimental removal percentage *versus* calculated values shown in Fig. 5 confirms the good fit of the predicted R^2 = 0.9659. Table 6 shows the optimum adsorption parameters optimized by CCD.

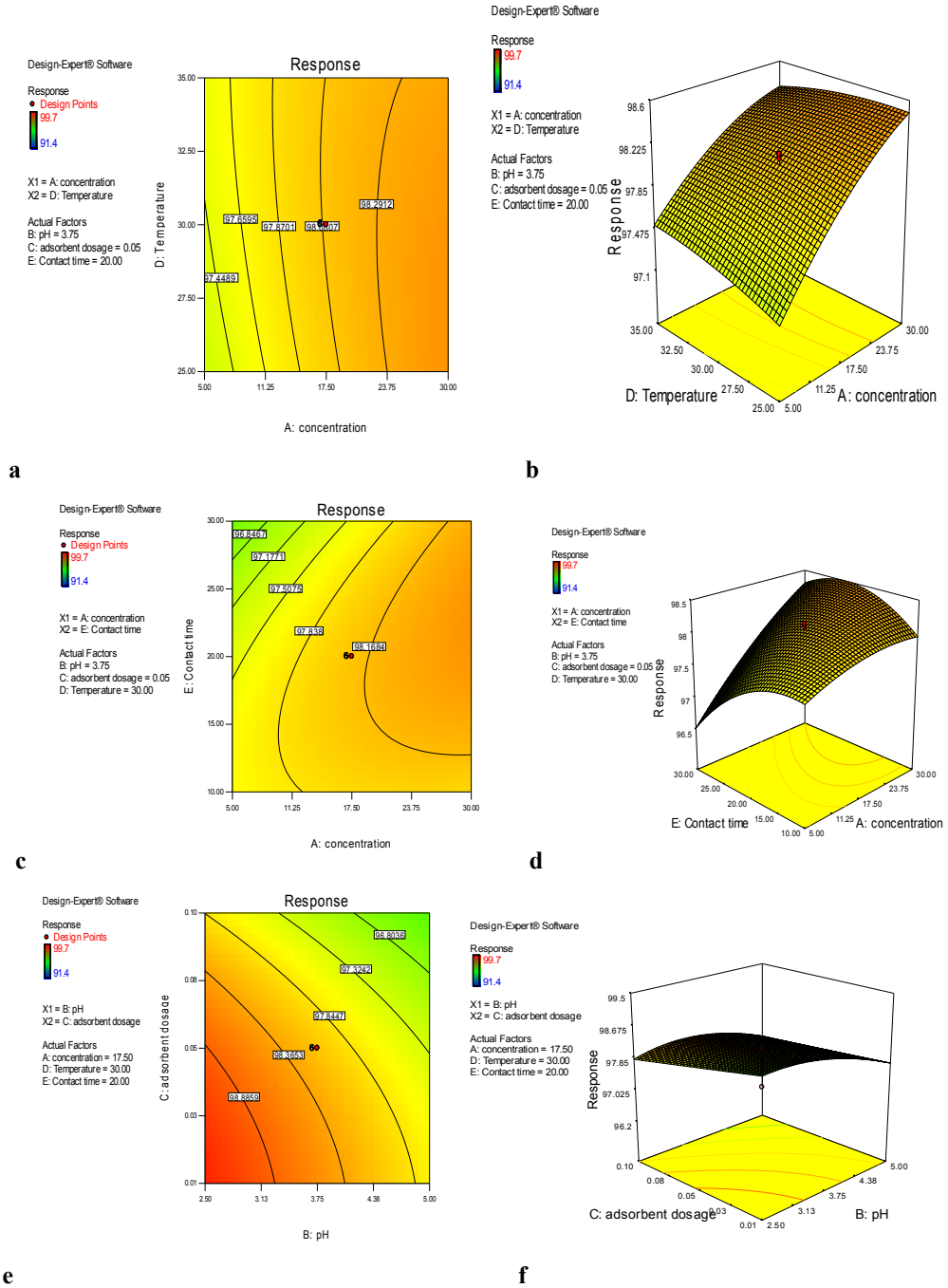

Fig. 5. The 3D surface and contour plots illustrating the interaction effects of the variables.

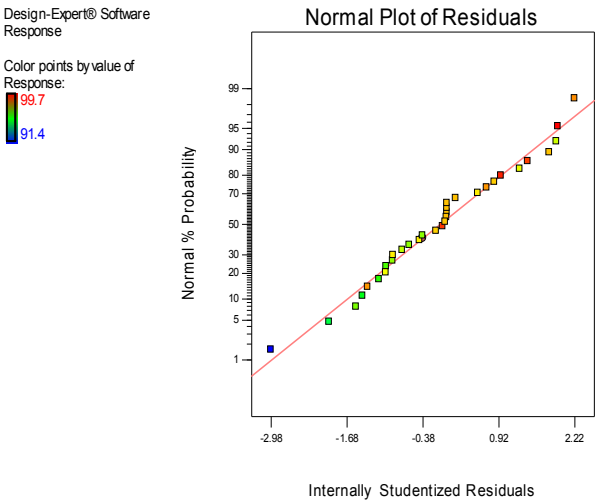

Fig. 6. The plot of experimental Allura Red removal percentage versus calculated values.

Equilibrium Isotherm Models

The experimental results related to the adsorption of Allura Red dye on the nanodiopside/Zn-Fe LDH composite were analyzed using Langmuir, Freundlich, and Temkin models. The Langmuir isotherm can be expressed as Eq. (3) [32]:

$$C_e/q_e = 1/q_{max} K_L + C_e/q_{max} \quad (3)$$

where q_e (mg g^{-1}) and C_e (mg l^{-1}) are the amounts of the adsorbed dye per unit mass of adsorbent and the unadsorbed dye concentration in solution at equilibrium, respectively. The q_{max} is the maximum amount of the Allura Red dye per unit mass of adsorbent (mg g^{-1}) on the surface bound at high C_e (mg g^{-1}), and K_L is the adsorption equilibrium constant (l mg^{-1}). Figure 7a shows the linear plot of C_e/q_e *vs.* C_e of Langmuir isotherm. The values of q_{max} and K_L were determined from the slope and intercepts of the plots and are presented in Table 7.

The Freundlich adsorption isotherm model can be applied for a multilayer heterogeneous adsorption and is expressed as Eq. (4) [33]:

$$\log q_e = 1/n \log C_e + \log K_F \quad (4)$$

where K_F (l g^{-1}) is the Freundlich isotherm constants that are related to maximum adsorption capacity and n is the intensity of adsorption. Figure 7b shows the linear plot

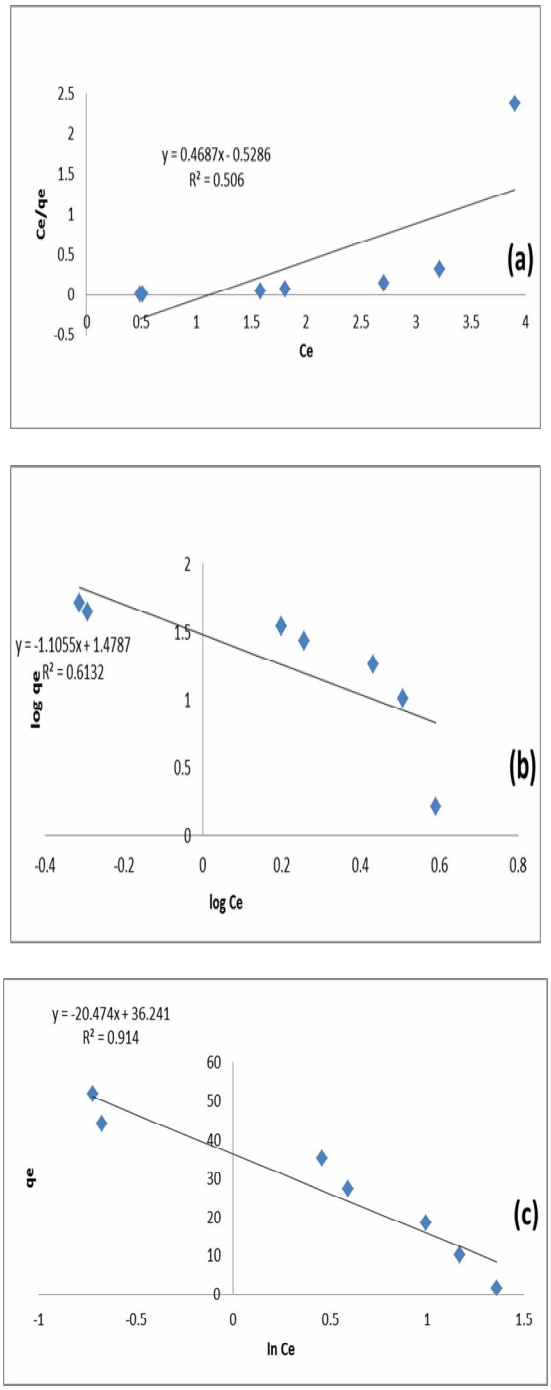

Fig. 7. The diagram of (a) Langmuir equilibrium isotherm, (b) Freundlich isotherm, and (c) Temkin isotherm.

($\log q_e$ *vs.* $\log C_e$) of the Freundlich isotherm. The plot of $\log q_e$ *vs.* $\log C_e$ was employed to generate the intercept value of K_F and the slope of $1/n_F$ (Table 7).

The adsorption enthalpy and the adsorbent-adsorbate interaction were studied by the Temkin isotherm model, which is expressed as Eq. (5) [34]:

$$q_e = B_t \ln K_T + B_t \ln C_e \quad (5)$$

where B_t is the Temkin constant related to the heat of the adsorption, T is the absolute temperature (K), and K_T is the equilibrium binding constant (l mg^{-1}). Figure 7c shows the linear plot of q_e *vs.* $\ln C_e$ of the Temkin isotherm model.

The constant parameters of isotherm equations and the correlation coefficient (R^2) for isotherm models are summarized in Table 7. The high correlation coefficient at various conditions shows the applicability of the Temkin model to experimental data.

Temkin noted that the heat of adsorption would more often decrease than increase with increasing coverage. The heat of adsorption (ΔH_{ad}) is defined as follows:

$$\frac{[A_{ad}]}{p_A[S]} = K_{eq}^{A} \propto e^{\frac{-\Delta G_{ad}}{RT}} = e^{\frac{\Delta S_{ad}}{R}} e^{\frac{-\Delta H_{ad}}{RT}}$$

In this model, it is assumed that as the surface is filled with adsorbate, the heat of adsorption of all the molecules in the layer would decrease linearly with coverage due to adsorbate-adsorbate interactions: $\Delta H_{ad} = \Delta H^{0}_{ad}(1-\alpha_T \theta)$, where α_T is a fitting parameter. In this isotherm, indirect adsorbate-adsorbate interactions are applied to adsorption isotherms [32].

Adsorption Kinetics

The kinetic analysis based on kinetic models, including pseudo first- and second-order, Elovich, and intraparticle diffusion models (Figs. 8a-d) provides good information about the rate and mechanism of adsorption. The obtained results of various kinetic models are summarized in Table 8. The highest R^2 value was observed in the pseudo-second-order kinetic model (0.9988), confirming the applicability of this model to experimental data.

Thermodynamic Study

In order to describe the thermodynamic adsorption behavior of Allura Red onto the nanodiopside/Zn-Fe LDH composite, thermodynamic parameters, including the change in free energy ($\Delta G_{ad}°$), enthalpy ($\Delta H_{ad}°$), and entropy ($\Delta S_{ad}°$), were calculated using the following thermodynamic equations (Table 9) [35]:

$$\Delta G° = -RT\ln K_c \quad (6)$$

$$\ln K_c = \Delta S°/R - \Delta H°/RT \quad (7)$$

where R is the universal gas constant (8.314 J K^{-1} mol^{-1}), T is the absolute solution temperature (K), and K_c is the equilibrium adsorption constant.

The plots of $\ln K_c$ *vs.* 1/T give a straight line from which $\Delta H_{ad}°$ and $\Delta S_{ad}°$ are calculated based on the slope and

Table 7. Isotherm Constant Parameters and Correlation Coefficients Calculated for the Adsorption of Allura Red onto the Nanodiopside/Zn-Fe LDH Composite

Isotherms	Equation	Parameters	Value
Langmuir	$\frac{C_e}{q_e} = \frac{1}{K_1 q_m} + \frac{C_e}{q_m}$	q_m (mg g^{-1})	-1.8918
		K_l (l mg^{-1})	4.0362
		R^2	0.5060
Freundlich	$\ln q_e = \ln K_f + \frac{1}{n}\ln C_e$	1/n	-1.1055
		$K_{f[}$ (mg g^{-1}) (l mg^{-1})$]^{1/n}$	30.1092
		R^2	0.6132
Temkin	$q_e = B_t \ln K_T + B_t \ln C_e$	Bt	-20.474
		K_T (l mg^{-1})	0.1703
		R^2	0.9140

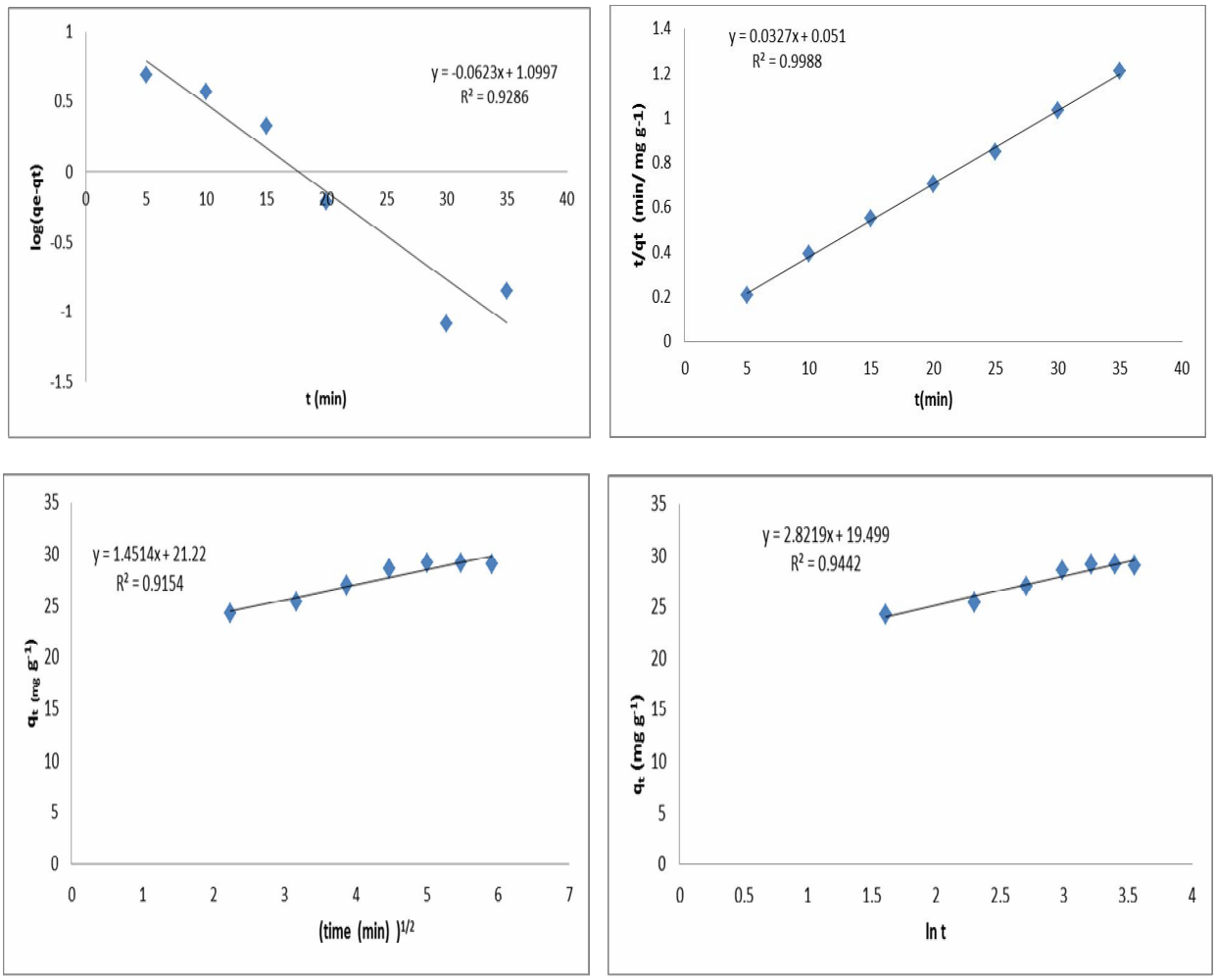

Fig. 8. The linear plot of the (a) pseudo-first-order kinetic, (b) pseudo-second-order kinetic, (c) intraparticle diffusion kinetic, and (d) Elovich kinetic models.

Table 8. Kinetic Parameters for the Adsorption of Allura Red onto Nanodiopside/Zn-Fe LDH Composite

Model	Equation	Parameters	Value
Pseudo-first-order	$\log(q_e - q_t) = \log(q_e) - \frac{k_1 t}{2.303}$	K_1 (min^{-1})	0.14
		R^2	0.9286
Pseudo-second-order	$\frac{t}{q_t} = \frac{1}{k_2 q_e^2} + \left(\frac{1}{q_e}\right)t$	k_2 (g mg^{-1} min^{-1})	0.02
		R^2	0.9988
Intraparticle diffusion	$q_t = K_{id}t^{1/2} + C$	K_{id}	1.45
		C	21.22
		R^2	0.9154
Elovich	$q_t = 1/\beta\ln(\alpha\beta) + 1/\beta\ln(t)$	β	0.35
		R^2	0.9442

Table 9. The Thermodynamic Parameters for the Sorption of Allura Red at Optimum Temperature

Thermodynamic parameters	Values (kJ mol^{-1})
-ΔH°	37.57
-TΔS°	8.20
-ΔG°	10.57
lnK_c	0.0352

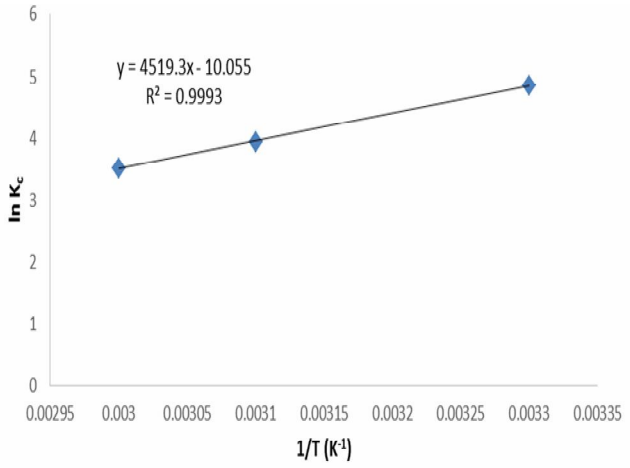

Fig. 9. The plots of lnK_c *vs*. 1/T.

intercept (Fig. 9). The negative $\Delta H_{ad}°$, -37.57 kJ mol^{-1}, confirms the physisorption mechanism of this adsorption process because this value is less than -40 kJ mol^{-1} [35].

The negative values of ΔG° indicate that the adsorption process was spontaneous and feasible at all the studied temperatures. In addition, the negative value of $\Delta S_{ad}°$ (-87.7 J mol^{-1} K^{-1}) suggests decreased randomness at the solid-solution interface during the adsorption process.

Reusability of Nanodiopside/Zn-Fe LDH Composite

In this study, the ability of the adsorbents to be used in several successive separation processes was examined. This was done to reuse the adsorbent for further successive cycles of the recovery process. For this purpose, first, all the parameters were optimized and the adsorption operation was performed. Then, the solution was strained, the amount of adsorption was read, and the precipitate under the filter for Allura Red was put in contact with pure ethanol. Afterward, they were filtered, and the precipitate was washed with distilled water and placed at room temperature to dry. In the next step, the deposition was used as the adsorbent of the second experiment. All these steps were repeated up to several consecutive cycles.

The obtained results showed that the nanodiopside/Zn-Fe LDH composite can be reused five times without any decrease in its efficiency.

Comparison with Other Studies

According to Table 10, a comparison between the adsorption capacities of adsorbent nanodiopside/Zn-Fe LDH and other adsorbents reported in the literature showed that the nanodiopside/Zn-Fe LDH composite had relatively a good adsorption capacity. Recyclability was investigated, and the results showed that the nanodiopside/Zn-Fe LDH composite could be an economical adsorbent candidate due to some advantages such as simplicity of operation, greenness, rapid sorbent, and cost-effectiveness, thus making it a suitable adsorbent for removal of other pollutants [35-45].

CONCLUSIONS

The objective of the present study was to find out the optimum parameters to maximize the adsorption of Allura Red by developing a model equation. The RSM model, using the CCD, was used based on five variables to determine both the individual and combined effects of different reaction variables, such as the initial concentration of Allura Red, pH, adsorbent dosage, temperature, and contact time. The regression analysis and optimization of variables were done using Design-Expert software to predict the response in all experimental regions. The experimental values were found to correspond well with those predicted by the model. The optimum production condition was found to include an initial Allura Red concentration of 19.8 mg l^{-1}, a pH value of 4.09, an adsorbent dosage of 0.04 g, a temperature of 32.61 °C, and a contact time of 23.93 min.

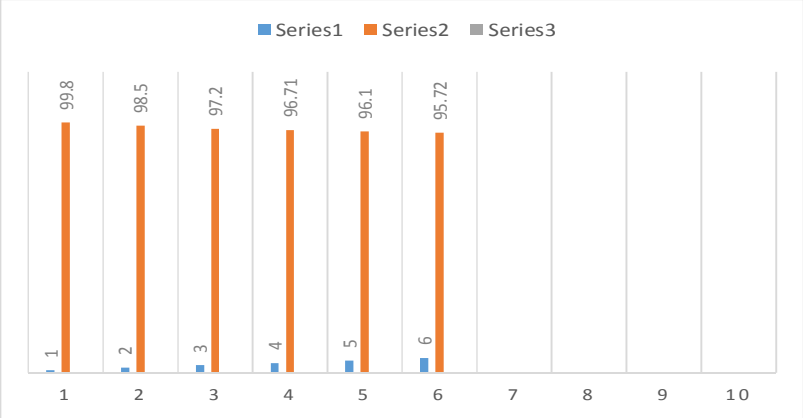

Fig. 10. The reusability of the nanodiopside/Zn-Fe LDH composite in five successive separation processes.

Table 10. A Comparison of the Maximum Sorption Capacity of Allura Red Dye on the Lichen Biosorbent with that of other Sorbents

Sorbent	Max sorption capacity	Ref.
α-Picoline ionic liquid-β-cyclodextrin-cross-linked polymer	0.0143	[35]
Activated pine wood	0.0143	[36]
Mn- and Cu-@ZnS nanoparticles loaded on activated carbon	0.101	[37]
Silica/AgNPs-glucose	0.136	[38]
Activated carbon	0.146	[39]
Poly(ionic liquid)immobilized magnetic nanoparticles	0.213	[40]
Spirulina platensis	0.944	[41]
Chitosan/polyurethane foam	0.217	[42]
Natural sawdust	0.051	[43]
Hexadecylpyridinium bromide treated sawdust	0.151	[44]
Pseudoevernia furfuracea biomass	0.280	[45]
Nanodiopside/Zn-Fe LDH composite	0.079	This work

ACKNOWLEDGEMENTS

The financial support of the research council of Payame Noor University of Isfahan is gratefully acknowledged.

REFERENCES

[1] Arica, T. A.; Ayas, E.; Arica, M. Y., Magnetic MCM-41 silica particles grafted with poly(glycidylmethacrylate) brush: modification and application for removal of direct dyes. *Microporous Mesoporous Mater.* **2017**, *243*, 164-175, DOI: 10.1016/j.micromeso.2017.02.011.

[2] Bayramoglu, G.; Altintas, B.; Arica, M. Y., Synthesis and characterization of magnetic beads containing aminated fibrous surfaces for removal of reactive green

19 dye: kinetics and thermodynamic parameters. *J. Chem. Technol. Biotechnol.* **2012**, *87*, 705-713, DOI: 10.1016/j.micromeso.2017.02.011.

[3] Cheng, Z.; Zhang, L.; Guo, X.; Jiang, X.; Li, T., Adsorption behavior of direct red 80 and congo red onto activated carbon/surfactant: process optimization, kinetics and equilibrium. *Spectrochim. Acta Part A Mol. Biomol. Spectroscop.* **2015**, *137*, 1126-1143, DOI: 10.1016/j.micromeso.2017.02.011.

[4] Vimonses, V.; Lei, S.; Jin, B.; Chow, C. W. K.; Saint, C., Adsorption of congo red by three Australian kaolins. *Appl. Clay Sci.* **2009**, *43*, 465-472, DOI: 10.1016/j.clay.2008.11.008

[5] Lawal, I. A.; Moodley, B., Synthesis, characterisation and application of imidazolium based ionic liquid modified montmorillonite sorbents for the removal of Allura Red dye, *RSC Adv.,* **2015**, *5*, 61913-61924, DOI: 10.1039/C5RA09483F

[6] Darmadi, Y., Mahidin, S. S.; Azzahra, M., Adsorption of mercury(II) ion in aqueous solution by using bentonite based monolith, *Key Engin. Mater.*, **2021**, *885*, 77-84, DOI: 10.4028/ www.scientific.net/KEM.885.7.

[7] Robinson, T.; McMullan, G.; Marchant, R.; Nigam, P., Remediation of dyes in textile effluent: a critical review on current treatment technologies with a proposed alternative. *Biores. Technol.* **2001**, *77*, 247-255, DOI: 10.1016/S0960-8524(00)00080-8.

[8] Rouquerol, J.; Rouquerol, F.; Llewellyn, P.; Maurin, G.; Sing, K., Adsorption by Powders and Porous solids, Second Ed., Academic Press, Amsterdam, **2014**.

[9] Do, D. D., Adsorption Science and Technology: Proceedings of the Second Pacific Basin Conference on Adsorption Science and Technology, World Scientific, Brisbane, **2000**.

[10] Ahmad, R.; Kumar, R., Adsorption of Allura Red dye onto alumina reinforced polystyrene clean-soil, *Air, Water* **2011**, *39*, 74-82, DOI: 10.1002/clen.201000125.

[11] Aguiar, J. E.; Bezerra, B. T. C.; Braga, B. D.; Lima, P. D. D.; Nogueira, R. E. F. Q.; de Lucena, S. M. P.; da Silva, I. J., Adsorption of anionic and cationic dyes from aqueous solution on non-calcined Mg-Al layered double hydroxide: experimental and theoretical study. *Sep. Sci. Technol.* **2013**, *48*, 2307-2316, DOI: 10.1080/01496395.2013.804837.

[12] Extremera, R.; Pavlovic, I., Perez, M. R.; Barriga, C., Removal of acid orange 10 by calcined Mg/Al layered double hydroxides from water and recovery of the adsorbed dye. *Chem. Eng. J.* **2012**, *213*, 392-400, DOI: 10.1016/j.cej.2012.10.042.

[13] Dos Santos, R. M. M.; Gonçalves, R. G. L.; Constantino, V. R. L.; da Costa, L. M.; da Silva, L. H. M.; Tronto, J.; Pinto, F. G., Removal of acid green 68:1 from aqueous solutions by calcined and uncalcined layered double hydroxides. *Appl. Clay Sci.* **2013**, *80*, 189-195, DOI: 10.1016/j.clay.2013.04.006.

[14] Bouhent, M. M.; Derriche, Z.; Denoyel, R.; Prevot, V.; Forano, C., Thermodynamical and structural insights of orange II adsorption by MgRAlNO$_3$ layered double hydroxides. *J. Solid State Chem.* **2011**, *184*, 1016-1024, DOI: 10.1016/j.jssc.2011.03.018.

[15] Woo, M. A.; Kim, T. W.; Paek, M. J.; Ha, H. W.; Choy, J. H.; Hwang, S. J., Phosphate-intercalated Ca-Fe-layered double hydroxides: Crystal structure, bonding character, and release kinetics of phosphate. *J. Solid State Chem.* **2011**, *184*, 171-176, DOI: 10.1016/j.jssc.2010.11.003.

[16] Wang, L.; Xu, X.; Evans, D. G.; Duan, X.; Li, D., Synthesis and selective IR absorption properties of iminodiacetic-acid intercalated MgAl-layered double hydroxide. *J. Solid State Chem.* **2010**, *183*, 1114-1119, DOI: 10.1016/j.jssc.2010.03.022.

[17] Baliarsingh, N.; Parida, K. M.; Pradhan, G. C., Influence of the nature and concentration of precursor metal ions in the brucite layer of LDHs for phosphate adsorption - a review. *RSC Adv.* **2013**, *3*, 23865-23878, DOI: 10.1039/c3ra42857e.

[18] Peter, M.; Kumar, P. T. S.; Binulal, N. S.; Nair, S. V.; Tamura, H.; Jayakumar, R., Development of novel α-chitin-nanobioactive glass ceramic composite scaffold for tissue engineering applications, *Carbohydr. Polym.* **2010**, *78*, *926* 2009. DOI: 10.1016/j.carbpol.2009.07.016.

[19] Jayakumar, R.; Menon, D.; Manzoor, K.; Nair, S.; Tamura, H., Biomedical applications of chitin and chitosan based nanomaterials -A short review. *Carbohydr. Polym.* **2010**, *82*, 227, DOI: 10.1016/ j.carbpol.2010.04.074.

[20] Choudhary, R.; Vecstaudza, J.; Krishnamurithy, G.; Raghavendran, H. R. B.; Murali, M. R.; T. Kamarul, T.; Swamiappan, S.; Locs, J., *In vitro* bioactivity ,biocompatibility and dissolution studies of diopside prepared from biowaste by using sol-gel combustion method. *Mater. Sci. Eng.* **2016**, *68*, 89, DOI: 10.1016/j.msec.2016.04.110.

[21] Rafiee, A.; Ghanavati Nasab, Sh.; Teimouri, A., Synthesis and characterization of pistachio shell/nanodiopside nanocomposite and its application for removal of crystal violet dye from aqueous solutions using central composite design. *Int. J. Environ. Anal. Chem.* **2019**, *1*, DOI: 10.1080/03067319.2019.1655556.

[22] Ghaedi, M.; Mazaheri, H.; Khodadoust, S.; Hajati, S.; Purkait, M., Application of central composite design for simultaneous removal of methylene blue and Pb^{2+} ions by walnut wood activated carbon. *Spectrochim. Acta, Part A* **2015**, 135, *479*, DOI: 10.1016/j.saa.2014.06.138.

[23] Bazrafshan, A.; Hajati,S.; Ghaedi, M., synthesis of regenrable $Zn(OH)_2$ nanoparticle loaded activated for the ultrasound-assisted removal malachite green:optimization, *Isotherm and Kinetics RSC Adv.* **2015** *5*, 79119, DOI: 10.1039/C5RA11742A.

[24] Ghaedi, M.; Ansari, A.; Sahraei, R., ZnS:Cu nanoparticles loaded on activated carbonas novel adsorbentfor kinetic, thermodynamic and isotherm studies of reactive Orange 12 and direct yellow 12 adsorption. *Spectrochim. Acta, Part A* **2013**, *114*, 687, DOI: 10.1016/j.saa.2013.04.091.

[25] Mahalik, K.; Sahu, J. N.; Patwardhan, A.; Meikap, B. C., Statistical modeling and optimization of hydrolysis of urea to generate ammonia for flue gas conditioning. *J. Hazard. Mater.* **2010**, *182*, 603-610, DOI: 10.1016/j.jhazmat.2010.06.075.

[26] Asfaram, A.; Ghaedi, M.; Abidi, H.; Javadian, H.; Zoladl, M.; Sadeghfar, F.; Synthesis of Fe_3O_4@CuS@Ni_2P-CNTs magnetic nanocomposite for sonochemical-assisted sorption and pre-concentration of trace Allura Red from aqueous samples prior to HPLC-UV detection: CCD-RSM design, *Ultrasonics-Sonochemistry*, **2018**, *44*, 240-250, DOI: 10.1016/j.ultsonch.2018.02.011.

[27] Schio, R. R.; Rosa, B.; Gonçalves Salau, N. P.; Mallmann, E. S.; Dotto, G. L., Fixed-bed adsorption of allura red dye on chitosan/polyurethane foam, *Chem. Eng. Technol.* **2019**, *42*, 2434-2442, DOI: 10.1002/ceat.201800749

[28] Ostovan, A.; Assadolahzadeh, H.; Ghaedi, M., Synthesis of Mn-and Cu-sound assisted extraction procedure and validation of a spectrophotometric method for a rapid preconcentration of Allura Red AC(E129) in food and water samples, *Ultrasonics-Sonochemistry*. **2018**, *43*, 53-60, DOI: 10.1016/j.ultsonch.2018.01.

[29] Ghorbanian, L.; Emadi, R.; Razavi, M.; Shin, H.; Teimouri, A., Synthesis and characterization of novel nanodiopside bioceramic powder. *J. Nanostruct.* **2012**, *2*, 357, DOI: 10.7508/JNS.2012.03.011.

[30] Abdel Moaty, S. A.; Farghali, A. A., Khaled, R., Preparation, characterization and antimicrobial applications of Zn-Fe LDH against MRSA. *Mater. Sci. Eng. C* **2016**, *68*, 184-193. DOI: 10.1016/j.msec.2016.05.110.

[31] Mao, H.; Ji, C. G.; Liu, M. H.; Sun, Y.; Liu, D. L.; Wu, S. Y.; Zhang, Y.; Song, X. M., Hydrophilic polymers/polypyrrole/graphene oxide nanosheets with different performance in electrocatalytic application to simultaneous determination of dopamine and ascorbic acid. *RSC Adv.* **2016**, *6*, 11632-11639, DOI: 10.1039/C6RA23341D.

[32] Al-Ghouti, M. A.; Da'ana, D. A., Guidelines for the use and interpretation of adsorption isotherm models: A review. *J. HazarD. Mater.,* **2020**, *393*, 122383, DOI: 10.1016/j.jhazmat.2020.122383.

[33] Citak, D.; Tuzen, M.; Soylak, M., Simultaneous coprecipitation of lead, cobalt, copper, cadmium, iron and nickel in food samples with zirconium(IV) hydroxide prior to their flame atomic absorption spectrometric determination, *Food and Chemical Toxicology* **2009**, *47*, 2302-2307, DOI: org/10.1016/j.fct.2009.06.021.

[34] Tempkin, M. J.; Pyzhev, V., Kinetics of ammonia synthesis on promoted iron catalysts. *Acta Physiochim. U.S.S.R.* **1940**, *12*, 217-222, DOI: 10.1021/j100120a035 I.

[35] Nandi, B. K.; Goswami, A.; Purkait, M. K., Adsorption

characteristics of brilliant green dye on kaolin. *J. Hazard. Mater.* **2009**, *161*, 387-395, DOI: 10.1016/j.jhazmat.2008.03.110.

[36] Qin, X.; Zhu, X., Determination of Allura Red in food by ionic liquid ß-cyclodextrin-cross-linked polymer solid phase extraction and high-performance liquid chromatography, *Anal. Lett.* **2016**, *49*, DOI: 10.1080/00032719.2015.1065880.

[37] Al-Ghouti, M. A.; Issa, A. A.; Al-Saqarat, B. S.; Al-Reyahi, A. Y.; Al-Degs, Y. S., Multivariate analysis of competitive adsorption of food dyes by activated pine wood Desalin. *Water. Treat.* **2016**, *57*, 27651-27662, DOI: 10.1080/19443994.2016.1174742.

[38] Ostovan, A.; Asadollahzadeh, H.; Ghaedi, M., Ultrasonically synthesis of Mn- and Cu-@ZnS-NPs-AC based ultrasound assisted extraction procedure and validation of a spectrophotometric method for a rapid preconcentration of Allura Red AC (E129) in food and water samples. *Ultrason. Sonochem.* **2018**, *43*, 52-60, DOI: 10.1016/j.ultsonch.2018.01.002.

[39] Salem, M. A.; Elsharkawy, R. G.; Ayad, M. I.; Elgendy, M. Y., Silver nanoparticles deposition on silica, magnetite, and alumina surfaces for effective removal of Allura red from aqueous solutions. *J. Sol-Gel Sci. Techn.* **2019**, *91*, 523-528, DOI: 10.1007/s10971-019-05055-7.

[40] Alkahtani, S. A.; Abu-Alrub, S. S.; Mahmoud, A. M., Adsorption of food coloring allura red dye (E129) from aqueous solutions using activated carbon. *Int. J. Food Apllied Sci.,* **2017**, *3*, 110-126, DOI: 10.21620/ijfaas.2017110-26.

[41] Bakheet, A. A. A.; Zhu, X. S., Poly(ionic liquid) immobilized magnetic nanoparticles as sorbent coupled with fluorescence spectrophotometry for separation/analysis of Allura Red. *J. Mol. Liq.* **2017**, *242*, 900-906, DOI: 10.1016/j.molliq.2017.07.097.

[42] Dotto, G. L.; Vieira, M. L. G.; Esquerdo, V. M.; Pinto, L. A. A., Equilibrium and thermodynamics of azo dyes biosorption onto Spirulina platensis. *Braz. J. Chem. Eng.* **2013**, *30*, 13-21, DOI: 10.1590/S0104-66322013000100003.

[43] da Rosa Schio, R.; Cruz da Rosa, B.; Salau, N. P. G.; Mallmann, E. S.; Dotto, G. L., Fixed-bed adsorption of Allura Red dye on chitosan/polyurethane foam. *Chem. Eng. Technol.* **2019**, *42*, 2434-2442. DOI: 10.1002/ceat.201800749.

[44] Saha, T. K.; Bishwas, R. K.; Karmaker, S.; Islam, Z., Adsorption characteristics of Allura Red AC onto sawdust and hexadecylpyridinium bromide-treated sawdust in aqueous solution. *ACS Omega*. **2020**, *5*, 13358-13374, DOI: 10.1021/acsomega.0c01493.

[45] Şeno, Z. M., Effective biosorption of Allura red dye from aqueous solutions by the dried-lichen (Pseudoevernia furfuracea) biomass, *Int. J. Environ Anal. Chem.* (In Press), DOI: 10.1080/03067319.2020.1785439.